The Journal of Experimental Medicine

MK2 controls the level of negative feedback in the NF-κB pathway and is essential for vascular permeability and airway inflammation

Magdalena M. Gorska,[1] Qiaoling Liang,[1] Susan J. Stafford,[2] Nicolas Goplen,[1] Nilesh Dharajiya,[2] Lei Guo,[1] Sanjiv Sur,[2] Matthias Gaestel,[3] and Rafeul Alam[1]

[1]Division of Allergy and Immunology, Department of Medicine, National Jewish Medical and Research Center, Denver, CO 80206
[2]Division of Allergy and Immunology, Department of Medicine, University of Texas Medical Branch, Galveston, TX 77555
[3]Institute of Biochemistry, Hannover Medical School, 30625 Hannover, Germany

We demonstrate that mitogen–activated protein kinase–activated kinase–2 (MK2) is essential for localized Th2-type inflammation and development of experimental asthma. MK2 deficiency does not affect systemic Th2 immunity, but reduces endothelial permeability, as well as adhesion molecule and chemokine expression. NF–κB regulates transcription of adhesion molecules and chemokines. We show that MK2 and its substrate HSP27 are essential for sustained NF–κB activation. MK2 and HSP27 prevent nuclear retention of p38 by sequestering it in the cytosol. As a result, MK2 precludes excessive phosphorylation of MSK1. By reducing MSK1 activity, MK2 prevents p65 NF–κB hyperphosphorylation and excessive IκBα transcription. IκBα mediates nuclear export of p65. By reducing IκBα level, MK2 prevents premature export of NF–κB from the nucleus. Thus, the MK2–HSP27 pathway regulates the NF–κB transcriptional output by switching the activation pattern from high level, but short lasting, to moderate–level, but long lasting. This pattern of activation is essential for many NF–κB–regulated genes and development of inflammation. Thus, the MK2–HSP27 pathway is an excellent target for therapeutic control of localized inflammatory diseases.

CORRESPONDENCE
Rafeul Alam:
alamr@njc.org

Abbreviations used: AHR, airway hyperresponsiveness; AU, arbitrary unit; BAL, bronchoalveolar lavage; BM, basement membrane; CREB, cAMP response element binding protein; ECM, extracellular matrix; EGF, epidermal growth factor; HE, hematoxylin and eosin; HUVEC, human umbilical vein endothelial cell; ICAM, intercellular adhesion molecule; MAPK, mitogen-activated protein kinase; MCP, monocyte chemoattractant protein; MK, MAPK-activated kinase; MNC, mononuclear cell; PAS, periodic acid-Schiff; VCAM, vascular cell adhesion molecule.

The development of inflammation depends not only on the immune response but also on an appropriate tissue response. Resident tissue cells play an essential role in inflammation by recruiting immune cells (1). The expression of adhesion molecules and the increase in permeability are two important changes that endothelial cells undergo to facilitate inflammation. Among many adhesion molecules, vascular cell adhesion molecule (VCAM)–1 plays a nonredundant role in Th2-type inflammation because of its selective recruitment of eosinophils and T cells (2). Endothelial permeability requires disassembly of intercellular junctions and cell shrinkage (3). These two processes are tightly linked to the actin cytoskeleton (4). The p38 mitogen-activated protein kinase (MAPK) is known to regulate many functions of endothelial cells (5–7). The p38

kinase activates several downstream effectors, and one of them is MAPK-activated kinase 2 (MK2; also known as MAPKAP-K2), which is a serine/threonine kinase (8). MK2 KO mice are resistant to endotoxic shock (9), which is a condition where endothelial cells play a prominent role. We hypothesize that MK2 regulates endothelial activities that are essential for development of inflammation.

RESULTS

MK2 KO mice are unable to increase vascular permeability in response to an allergen challenge

We studied the role of MK2 in vascular permeability and inflammation in a murine model of asthma using MK2 KO animals. MK2 KO and littermate (129/C57BL/ 6) control mice were immunized with and exposed to OVA, as previously described (10). We examined pulmonary

vascular permeability for Evans blue dye after an allergen challenge (11). Vascular permeability was significantly decreased ($P < 0.05$ for each time point after challenge) in MK2 KO mice compared with immunized and challenged control mice (referred to as control mice hereafter; Fig. 1 A) and was identical to that in nonimmunized mice. Thus, MK2 KO mice are unable to increase vascular permeability in response to the allergen.

MK2 KO mice do not increase actin polymerization and disrupt endothelial adherens junctions in response to an allergen challenge

Formation of intercellular gaps is essential for increased permeability. It requires endothelial cell shrinkage through actin polymerization (1, 4). Pulmonary vascular endothelial cells from control mice showed significantly ($P = 0.012$) increased actin polymerization (Fig. 1 B and Fig. S1, available at
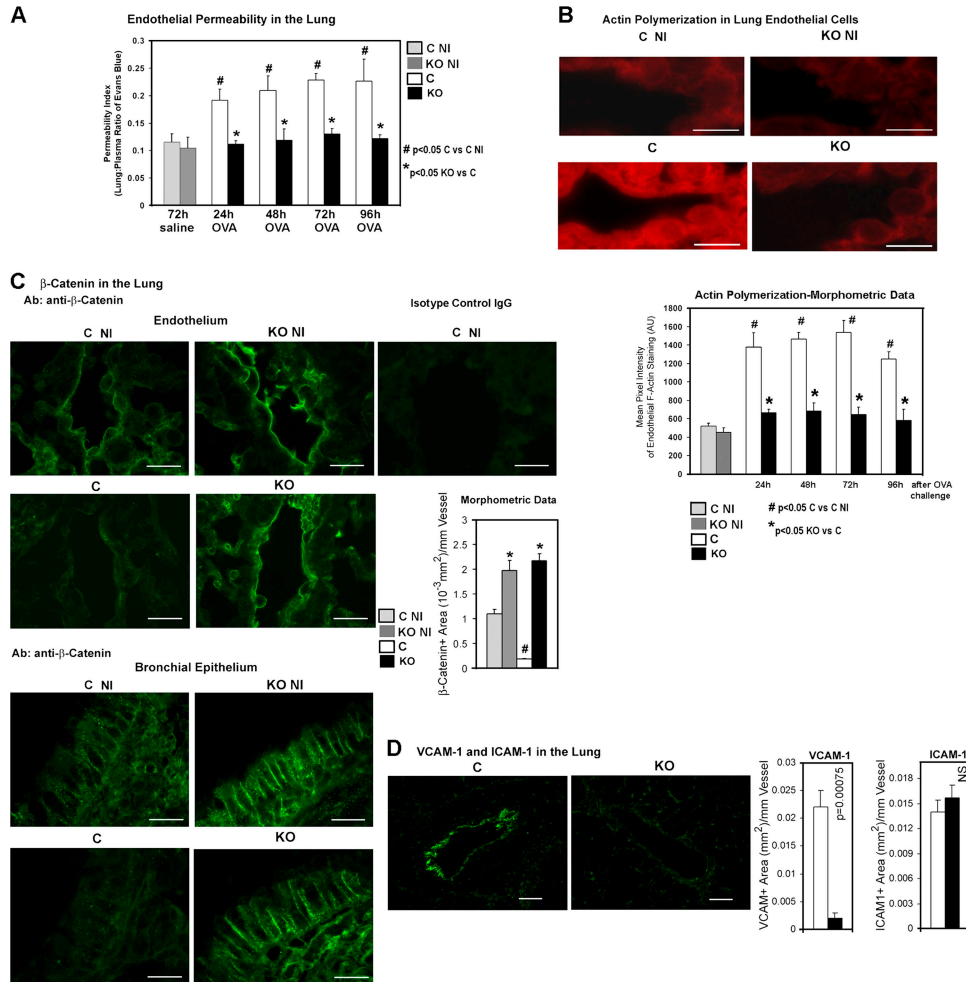

Figure 1.   Pulmonary endothelium in MK2 KO mice. (A) MK2 knockout mice (KO, black bar) and their littermate controls (C, open bar) were immunized and challenged with OVA. Nonimmunized (alum-injected), saline-challenged MK2 knockout (KO NI, dark gray bar), and littermate control (C NI, light gray bar) mice were also studied. Pulmonary vascular permeability was assessed. 24, 48, 72, or 96 h after OVA challenge, mice were i.v. injected with Evans blue dye. Next, a blood sample was taken and lungs were removed. The histogram shows the mean ratio between the amount of the dye extracted from 100 mg of the lung tissue and the amount of the dye extracted from 100 μl of plasma (lung/plasma ratio of Evans Blue dye = permeability index). Error bars show the SEM ($n = 5$ mice per group). (B) Lung sections from immunized mice obtained 24, 48, 72, and 96 h after OVA challenge or from nonimmunized mice were stained with rhodamine-labeled phalloidin to detect polymerized actin (red). The pictures show staining of pulmonary endothelium from immu- nized mice 24 h after OVA challenge and from nonimmunized mice. The histogram to the right shows mean pixel intensity of endothelial cell staining (blood vessels with a lumen perimeter of 0.1–1.5 mm; $n = 3$ mice per group). Intensity is expressed in arbitrary units (AU). (C) Lung sections from mice treated as in A were immunostained for β-catenin (green). Lung sections from control nonimmunized (C NI) mice were also stained with isotype control IgG. The graph shows mean immunostained area per mm of blood vessel with a lumen perimeter of 0.1–1.5 mm ($n = 3$ mice per group). Ab, antibody. (D) Lung sections from immunized and challenged mice (as in A) were stained with anti–VCAM-1 (green) or anti–ICAM-1 (staining not depicted) antibodies. Histograms show mean immunostained area per millimeter of blood vessel with a lumen perimeter of 0.1–1.5 mm ($n = 3$ mice per group). NS, statistically not significant. Bars: (B and C) 10 μm; (D) 20 μm.

http://www.jem.org/cgi/content/full/jem.20062621/DC1) compared with nonimmunized animals. In contrast, MK2 KO mice showed a twofold reduction (P = 0.006) in endothelial actin polymerization. In agreement with our results, a recent paper demonstrated reduced actin polymerization in endothelial cells overexpressing a dominant-negative MK2 (12).

β-catenin is an essential component of adherens junctions, and it normally stains the cellular border (1). β-catenin knockout endothelial cells have increased permeability (13). An allergen challenge of control mice caused disappearance of junctional β-catenin, indicating a disruption of adherens junction (Fig. 1 C). In contrast, MK2 KO mice showed an overall increase in β-catenin staining along the cell border.

Impaired VCAM–1 expression, inflammatory cell accumulation, and Th2 cytokine production in the lung from MK2 KO mice

Lung endothelium from MK2 KO mice showed a 10-fold reduction (P = 7.5×10^{-4}) in VCAM-1 expression compared with control mice (Fig. 1 D). Intercellular adhesion molecule (ICAM)–1 expression was similar in both groups. Control mice demonstrated pronounced peribronchial inflammation after the allergen challenge (Fig. 2 A). The mean peribronchial inflammatory area was reduced by 7.5-fold in MK2 KO mice (P = 0.0018). Furthermore, MK2 KO mice demonstrated a significant (P = 9.4×10^{-5}) reduction in the total number of bronchoalveolar lavage (BAL) cells (Fig. 2 B). The percentage of eosinophils in the BAL fluid from control mice was 37 ± 5%, but only 9 ± 3% in MK2 KO mice (P = 0.04).

The profound reduction in the eosinophil number in the lung from MK2 KO mice suggested an impaired Th2 immunity. In agreement, Th2 cytokine mRNA was expressed at a reduced level in the lung from MK2 KO mice, as follows: IL-4 (fourfold reduction, P = 0.016), IL-5 (3.7-fold reduction, P = 0.042), IL-10 (twofold reduction, P = 0.042), and IL-13 (twofold reduction, P = 0.029; Fig. 2 C).

Mucus production, extracellular matrix (ECM) protein deposition, airway smooth muscle hypertrophy, and airway hyperresponsiveness (AHR) in MK2 KO mice

Thickening of the smooth muscle layer, mucus, and ECM overproduction are important consequences of airway allergic inflammation. MK2 KO mice showed a profound reduction in all of the aforementioned aspects of tissue remodeling (Fig. S2, A–C, available at http://www.jem.org/cgi/content/full/jem.20062621/DC1). The basal function of lung-resident cells is regulated by tissue-derived factors, such as epidermal growth factor (EGF) (14, 15). The staining with an anti–phospho-EGF receptor antibody (Tyr1173) was equally intensive in MK2 KO and control mice (Fig. S2 D). AHR was assessed by measuring total lung resistance to increasing doses of methacholine (Fig. 2 D). OVA challenge of control mice resulted in an increase in lung resistance starting at the lowest methacholine dose and reaching a 9.4-fold increase over baseline at the highest dose. The airway resistance of MK2 KO mice was significantly lower at each methacholine dose compared with control mice (Student's t test, P < 0.04 for each methacholine dose; repeated measures ANOVA, P = 0.0004 for the entire dose–response curve).
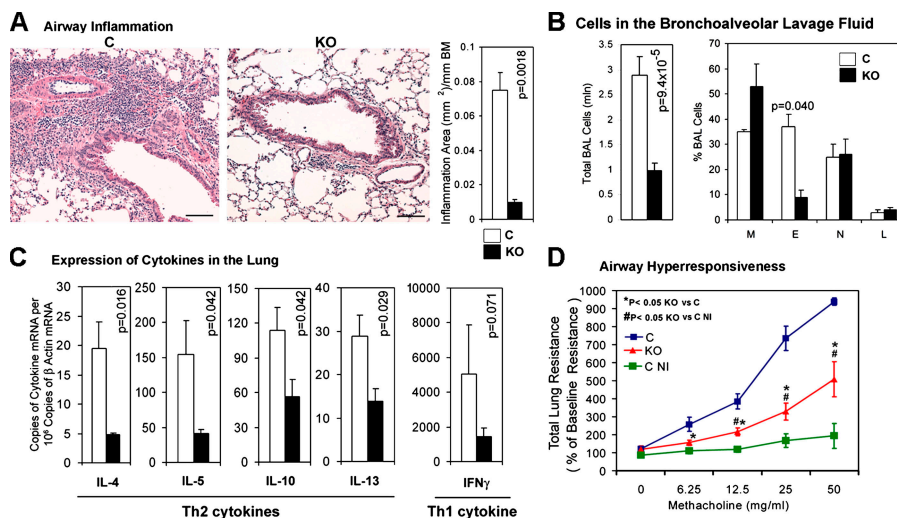

Figure 2.   Local (airway) immune response in MK2 KO mice. (A) Lung sections from immunized and challenged mice (as in Fig. 1 A) were stained with HE. Bars, 100 μm. Histogram shows mean area of inflammation per millimeter of BM of mid-size bronchi (BM perimeter range 0.4–2.0 mm; n = 6 mice per group). (B) The left histogram presents the mean number of BAL cells. The right histogram shows the cellular composition of the BAL fluid. The mean number of macrophages (M), eosinophils (E), neutrophils (N), and lymphocytes (L) is displayed as a percentage of the total cell number (n = 8 mice for C group and 10 mice for KO group). (C) RNA was extracted from lungs obtained from mice treated as in Fig. 1 A. Cytokine and β-actin mRNA was quantified by real-time RT-PCR. Histograms show mean number of cytokine mRNA copies per 10^6 copies of β actin mRNA (n = 3 mice per group). (D) Immunized and challenged control and KO (as in Fig. 1 A), as well as nonimmunized control (C NI) mice were exposed first to saline aerosol, and then to increasing concentrations of methacholine, and total lung resistance was measured. Baseline resistance was obtained before any aerosol administration (n = 5 mice per C and KO group; n = 3 mice per C NI group). Error bars represent the SEM.
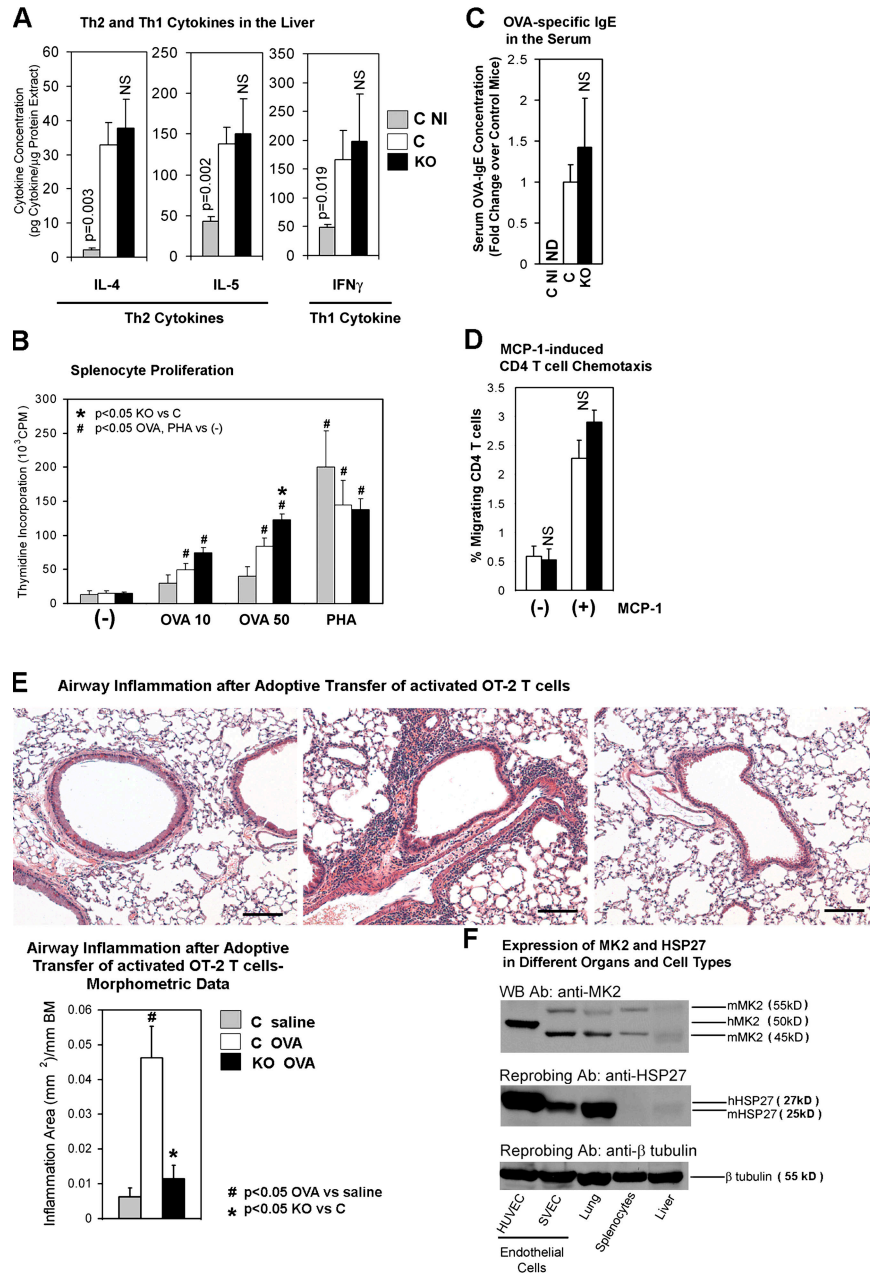
Figure 3. Systemic immune response in MK2 KO mice. (A) Cytokine concentration in the liver lysate from immunized mice (KO and C) and nonimmunized control mice (C NI, gray bar) was measured by ELISA (each experiment in duplicates, $n = 3$ mice per group). Values were adjusted for the protein concentration in the lysate. (B) Splenocytes from mice as in Fig. 1 A were stimulated with 10 or 50 μg/ml OVA (OVA 10 or OVA 50) or PHA at 5 μg/ml. [³H]thymidine incorporation was measured (experiment in triplicates; $n = 4$ mice per C group; $n = 6$ mice per KO group; $n = 3$ mice per C NI group). CPM, counts per minute. (C) Mice were treated as in Fig. 1 A. OVA-specific IgE in the serum was measured by ELISA (each experiment in duplicates; $n = 3$ mice per C or C NI group; $n = 5$ mice per KO group). ND, not detected. (D) CD4 T cells were isolated from the spleen of immunized mice (as in Fig. 1 A) and assayed for chemotaxis toward MCP-1. The histogram shows the percentage of migrated CD4 T cells (experiment in duplicates; $n = 3$ mice per group). (E) Mice were injected i.v. with OVA peptide-activated OT-2 T cells and exposed to OVA or saline aerosol. Airway inflammation was measured as in Fig. 2 A. C saline, saline-exposed control mice; C OVA or KO OVA, OVA-exposed control or MK2 KO mice, respectively ($n = 3$ mice per group). Bars, 100 μm. (F) Lysates from organs obtained from nonimmunized wild-type (C57BL/6) mice and from human (HUVEC) and mouse (SVEC) endothelial cells were Western blotted with an anti-MK2 antibody, followed by sequential reprobing with anti-HSP27 and anti–β-tubulin antibodies. hMK2, human MK2; mMK2, murine MK2; hHSP27, human HSP27; mHSP27, murine HSP27. Error bars represent the SEM.

Systemic T helper immunity in MK2 KO Mice

We wondered if MK2 KO mice had a systemic defect in cytokine production. We measured T helper cytokines in a different organ, i.e., liver by ELISA. IL-4, IL-5, and IFNγ levels in the liver homogenates from MK2 KO and control mice were similar and 3.2–14.3-fold higher than levels in the non-immunized group (Fig. 3 A). OVA-stimulated proliferation of splenocytes from MK2 KO mice was slightly higher than that from control mice (Fig. 3 B). PHA-stimulated proliferation was similar in both groups. The OVA-specific IgE levels in the serum from MK2 KO and control mice were similar (Fig. 3 C). Monocyte chemoattractant protein (MCP)–1–directed, as well as spontaneous, migration of MK2 KO and control CD4 T cells were similar (Fig. 3 D). Adoptively transferred, activated, OVA-specific, MK2-sufficient OT-2 T cells were unable to reconstitute airway inflammation in MK2 KO mice in response to OVA aerosol challenge (Fig. 3 E) (16). They induced considerable airway inflammation in control mice. Finally, the eosinophil counts in the peripheral blood from control and MK2 KO mice were equal (∼2%). Thus, lack of allergic inflammation in MK2 KO mice cannot be attributed to the impairment of the systemic T helper response.

The expression of MK2 protein and its substrate HSP27 was considerably lower or minimally present, respectively, in splenocytes compared with endothelial cells or lung, and the expression was almost undetectable in the liver (Fig. 3 F).

This low-level expression is the likely explanation for the relatively unperturbed function of lymphocytes from the blood, spleen, and liver from MK2 KO mice.

Production of TNFα and chemokine in MK2 KO mice

TNFα is a master regulator of inflammation, and its synthesis is regulated by the p38 pathway (17, 18). TNFα production was shown to be decreased in LPS-stimulated MK2 KO spleen cells in a previous study (9). The TNFα mRNA level in the lung and TNFα protein level in the liver from immunized MK2 KO mice were similar to those in control mice (Fig. 4 A). The discrepancy between the abovementioned study and our data might be the result of the differences in the stimulus and model used. We examined representative chemokine expression in the lung (Fig. 4 B). The expression of MCP-1, MCP-3, and eotaxin mRNA in KO mice was reduced by 3.1- (P = 6.3 × 10⁻⁴), 3.8- (P = 0.016), and 1.9-fold (P = 0.034), respectively. We believe that the reduction in inflammatory cells and cytokines in the MK2 KO lung is the result of aberrant endothelial function, defective chemokine expression, and faulty cell recruitment into the airways.

Reduced allergic inflammation after administration of a neutralizing anti–VCAM-1 antibody

We wondered if a perturbation in endothelial function in wild-type mice could reproduce the MK2 phenotype.
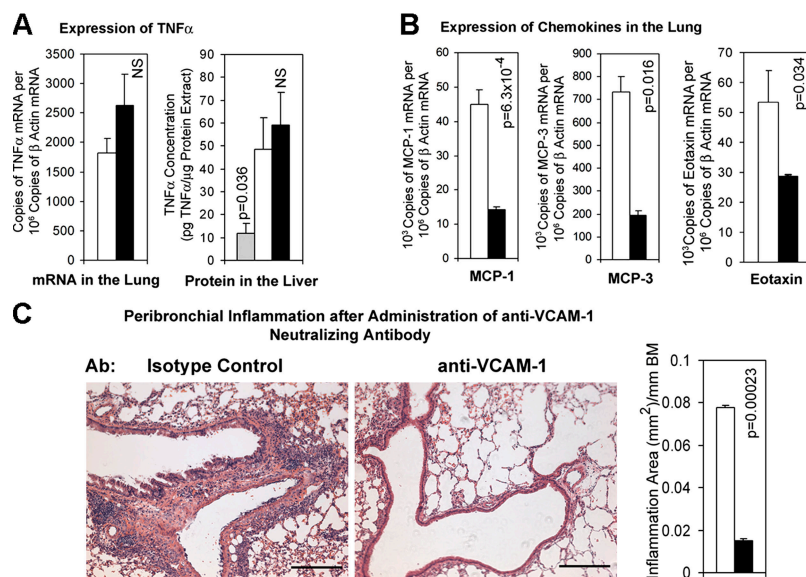

Figure 4. Other mechanisms of leukocyte recruitment to the lung of MK2 KO mice. (A, left) TNFα and β-actin mRNA in the lung was quantified by real-time RT-PCR, as in Fig. 2 C. The histogram shows the mean number of TNFα mRNA copies per 10⁶ copies of β-actin mRNA (n = 3 mice per group). (right) The concentration of TNFα in the liver lysate was measured by ELISA as in Fig. 3 A (each experiment in duplicates, n = 6 mice for the control group, 8 mice for the KO group, and 3 mice for the C NI group). (B) MCP-1, MCP-3, eotaxin, and β-actin mRNA in the lung was quantified by real-time RT-PCR as in Fig. 2 C. The histograms show mean copies of MCP-1 (left), MCP-3 (middle), and eotaxin (right) mRNA per 10⁶ copies of β actin mRNA (n = 3 mice per group). (C) Wild-type mice (C57BL/6) were immunized with OVA as in Fig. 1 A and pretreated i.v. with 10 mg/kg neutralizing anti–VCAM-1 antibody or isotype control antibody (Ab), followed by OVA challenge. Lung sections were stained with HE, and the airway inflammation was measured as in Fig. 2 A (right, n = 2 mice per group). Bars, 200 μm. Error bars represent the SEM.
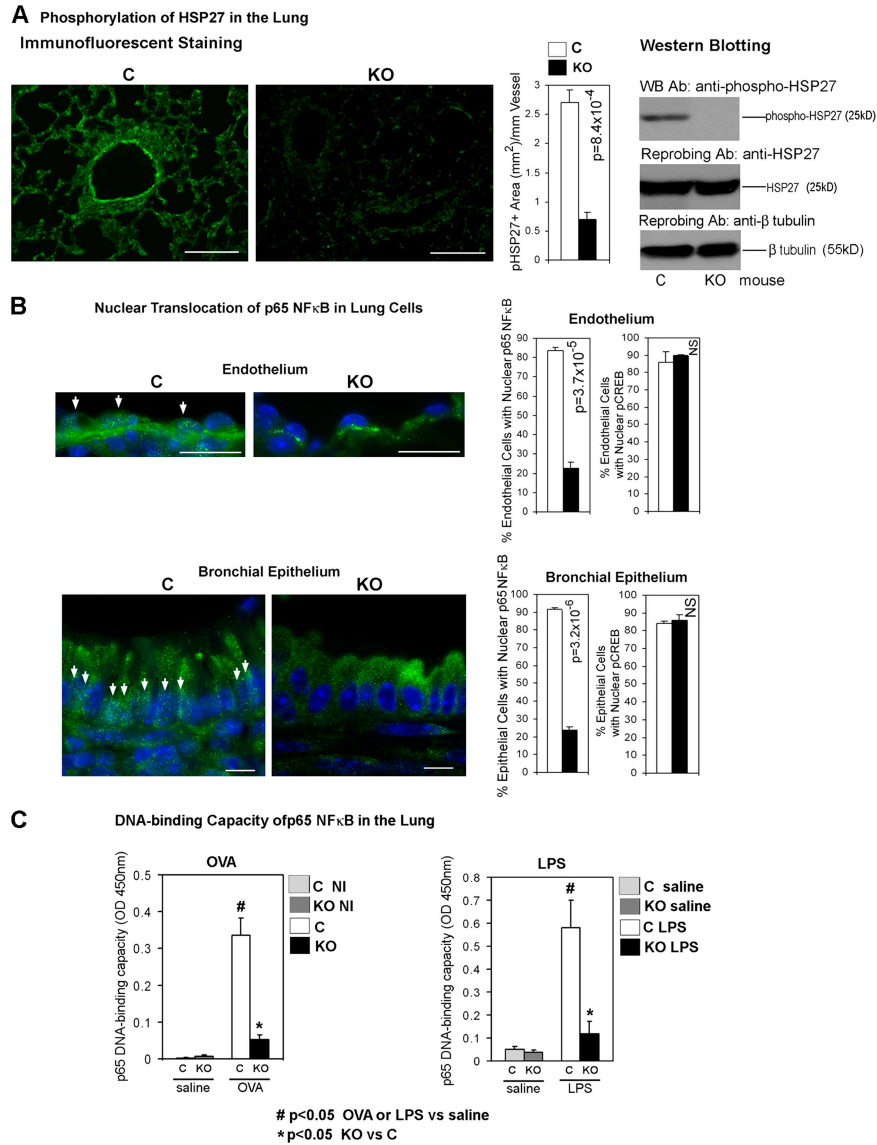
A Phosphorylation of HSP27 in the Lung
Immunofluorescent Staining

Western Blotting

B Nuclear Translocation of p65 NFκB in Lung Cells

C DNA-binding Capacity ofp65 NFκB in the Lung

# p<0.05 OVA or LPS vs saline
* p<0.05 KO vs C

Figure 5. Nuclear targeting of NF–κB in the lung of MK2 KO mice. (A, left) Lung sections from immunized and challenged mice (as in Fig. 1 A) were stained with an anti–phospho-HSP27 (Ser15) antibody (green). The histogram shows mean phospho-HSP27–positive (pHSP27+) area per millimeter of blood vessel perimeter (lumen perimeter range, 0.1–1.5 mm; $n = 3$ mice per group). (A, right) Lung lysates from immunized and challenged mice (as in Fig. 1 A) were Western blotted with an anti–phospho-HSP27 (Ser15) antibody. The membrane was reprobed with an anti-HSP27 and, next, with an anti–β-tubulin antibody. (B) Lung sections from immunized and challenged mice (as in Fig. 1 A) were stained with DAPI (staining nucleus in blue) and an antibody against the p65 subunit of NF-κB (green) or phospho-CREB (Ser133, staining not depicted). Arrows indicate p65 NF-κB–positive nuclei. Histograms show mean percentage of endothelial and epithelial cells showing nuclear p65 NF-κB (left; $n = 3$ mice per group) or pCREB (right; $n = 3$ mice per group). (C, left) Mice were immunized and challenged with OVA as in Fig. 1 A. (C, right) Naive nonimmunized mice were intranasally exposed to LPS (as a positive control for NF-κB activation) or saline. The DNA-binding capacity of p65 in lung nuclear extracts was measured using the TransAM NF-κB p65 ELISA kit (Active Motif; $n = 3$). (right) Black (KO LPS) or dark gray (KO saline) bars, MK2 knockout administered with LPS or saline, respectively; open (C LPS) or light gray (C saline) bars, littermate control mice administered with LPS or saline, respectively. Bars: (A) 50 μm; (B, top) 10 μm; (B, bottom) 5 μm. Error bars represent the SEM.

OVA-immunized wild-type mice were pretreated with a neutralizing anti–VCAM-1 antibody before an inhalation challenge. We observed a 5.2-fold ($P = 2.3 \times 10^{-4}$) reduction in peribronchial inflammation in anti-VCAM-1–pretreated mice compared with mice pretreated with the control IgG (Fig. 4 C).

Reduced phosphorylation of HSP27 and nuclear translocation of p65 NF–κB in MK2 KO mice

NF-κB is an important transcriptional regulator of VCAM-1 gene (19, 20). Among the MK2-regulated proteins, HSP27 and Akt have been linked to the activation of NF-κB (21–23).

HSP27 has actin-capping activity, which is inhibited by its phosphorylation (24). There was no difference in the lung staining pattern of phosphorylated Akt (Ser438, which is an MK2 phosphorylation site) between KO and control mice (unpublished data). In contrast, HSP27 phosphorylation (Ser15, which is an MK2-specific HSP27 phosphorylation site [25]) was reduced by 3.6-fold (P = 8.4×10^{-4}) in MK2 KO mice (Fig. 5 A). The reduction was most prominent in pulmonary vascular endothelial cells. Next, lung tissue was examined for nuclear p65 NF-κB and, as a control, nuclear phospho–cAMP response element binding protein (CREB; Ser133) (Fig. 5 B). MK2 KO mice showed reduced nuclear p65, but not phospho-CREB, in most cells in the lung. We quantified nuclear p65 in endothelial and bronchial epithelial cells because the expression of NF-κB–dependent molecules (VCAM-1 and chemokines, respectively) was decreased in these cells (20). The number of endothelial and bronchial epithelial cells with nuclear p65 was reduced by
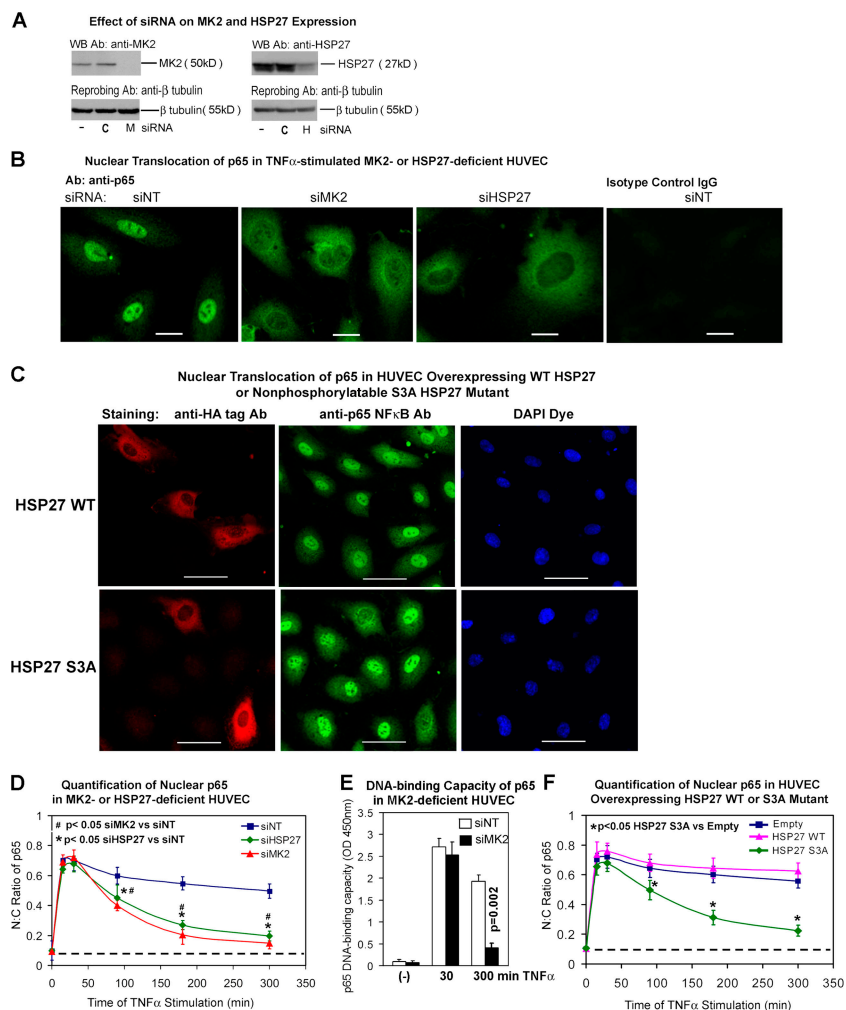

Figure 6. Nuclear targeting of NF–κB after inhibition of MK2 or HSP27 in endothelial cells. (A) HUVECs were treated with Lipofectamine 2000 alone (−), Lipofectamine 2000 plus control, nontargeting siRNA (C), or siRNA against MK2 (M) or HSP27 (H). Cell lysates were Western blotted with anti-MK2 (left) or anti-HSP27 (right) antibodies (Ab). The membrane was reprobed with an anti–β-tubulin antibody. (B and D) HUVECs transfected as in A were stimulated with TNFα for 15, 30, 90, 180, or 300 min, or left unstimulated. Next, cells were immunostained for p65. siNT-transfected cells were also stained with isotype control IgG. (B) The images show p65 staining of cells stimulated with TNFα for 5 h. Only two HSP27-deficient cells are shown because of the increased size (Fig. 10 A). Bar, 10 μm. The integrated intensity of cytoplasmic and nuclear p65 staining was measured. (D) The graph shows nuclear to cytoplasmic (N:C) ratio of p65 staining intensity at each time point of TNFα stimulation (n = 10–20 representative cells from 3 separate experiments). The dashed line represents the baseline (no TNFα) N:C ratio. (C and F) HUVECs transfected with the empty vector (Empty) or vector containing an HA-tagged wild-type HSP27 cDNA (HSP27 WT) or HA-tagged mutant HSP27 (Ser15,78,82Ala = S3A) were stimulated as in B, immunostained for the HA-tag (red) and p65 (green), and treated with DAPI (staining nuclei in blue). Images of cells at 5 h of stimulation are shown in C. Bars, 25 μm. (F) The N:C ratio was measured as in D. Only HA-positive cells (HSP27 WT and HSP27 S3A) were assessed. The dashed line represents the baseline (no TNFα) N:C ratio (n = 10–20 representative cells from 3 separate experiments). (E) HUVECs transfected with siRNA for MK2 (siMK2, filled bars) or nontargeting siRNA (siNT, open bars) were stimulated with TNFα for 30 or 300 min, or left unstimulated (−). The DNA-binding capacity of p65 in nuclear extracts was assessed as in Fig. 5 C (n = 3). Error bars represent the SEM.

3.7- (P = 3.7 × 10⁻⁵) and 3.9-fold (P = 3.2 × 10⁻⁶), respectively. We measured the DNA-binding capacity of NF-κB in nuclear extracts from the lung of MK2 KO and control mice (Fig. 5 C). We used an ELISA-based TransAM NF-κB Activation kit (26–28). The advantage of this ELISA-based approach over the traditional EMSA is that the former provides quantitative results. To induce NF-κB activation in the lung, mice were intranasally challenged with OVA or LPS (positive control). Both OVA and LPS treatment substantially increased the DNA-binding capacity of p65 in the lung of control mice. The DNA-binding capacity of p65 in OVA- and LPS-treated MK2 KO mice was reduced by 6.5- and 5-fold, respectively, compared with control mice. We checked the specificity of the assay. Soluble competitor oligonucleotides containing the wild-type or mutated NF-κB consensus-binding site were added in excess to the nuclear extract from LPS-treated control lung. The wild-type oligo prevented NF-κB binding to the immobilized probe (OD 450 nm = 0.044 ± 0.014). The mutated oligo had no effect (OD 450 nm = 0.568 ± 0.131).

Impaired nuclear retention of p65 in MK2– and HSP27–deficient endothelial cells

To determine their role in NF-κB regulation, we performed MK2 and HSP27 knockdown experiments (Fig. 6 A) in human umbilical vein endothelial cells (HUVECs). MK2, HSP27, or nontargeting siRNA-transfected HUVECs were stimulated with TNFα and then immunostained for p65 (Fig. 6 B). At early time points (15 and 30 min), the nuclear/cytoplasmic ratio of p65 was similar in all study groups (Fig. 6 D). At later time points, cells transfected with MK2 or HSP27 siRNA demonstrated an accelerated loss of p65 from the nucleus. Therefore, MK2 or HSP27-deficient cells have the ability to translocate p65 to the nucleus at a normal rate, but are unable to sustain it in this location. Interestingly, we noticed that the size of HSP27-deficient HUVECs was considerably increased. We speculate that it is caused by an abnormal cytoskeleton because HSP27 is a known regulator of actin polymerization. We also measured NF-κB activation in nuclear extracts from transfected HUVECs (Fig. 6 E). At an early time point (30 min) of TNFα stimulation, the DNA-binding capacity of p65 was similar in siNT and siMK2-transfected cells. However, at a late time point (5 h), siMK2-transfected cells demonstrated a 4.7-fold reduction in the DNA-binding capacity of p65.

Impaired nuclear retention of p65 in cells expressing a nonphosphorylatable mutant of HSP27

MK2 phosphorylates HSP27 at serine 15, 78, and 82 (29). We asked if this phosphorylation was necessary to maintain p65 in the nucleus after TNFα stimulation. HUVECs were transfected with a nonphosphorylatable mutant of HSP27 (Ser15,78,82Ala), wild-type HSP27, or empty vector (Fig. 6 C). The kinetics of p65 nuclear localization in mutant HSP27-expressing cells resembled that in HSP27-deficient cells (Fig. 6 F), suggesting a necessary role for HSP27 phosphorylation.

Reversal of impaired nuclear retention of p65 by leptomycin B

We examined the mechanism of shortened nuclear presence of NF-κB. MK2- or HSP27-deficient cells and control cells were treated with the CRM1 inhibitor leptomycin B before TNFα stimulation. CRM1, which is an exportin-type nuclear chaperone, exports NF-κB back to the cytosol (30). Pretreatment with leptomycin B caused remarkable nuclear accumulation of p65 in both MK2- and HSP27-deficient cells (Fig. 7 A). The results indicate that accelerated nuclear export is the primary cause of reduced nuclear p65.

Increased IκBα in cells transfected with MK2 or HSP27 siRNA

NF-κB is exported from the nucleus with the help of newly synthesized IκBα (31, 32). This occurs because IκBα is one of the first target genes of NF-κB. The IκBα level in unstimulated MK2- or HSP27-deficient cells was comparable to that in control cells (Fig. 7 B). 15 min of TNFα stimulation resulted in the disappearance of IκBα protein in all 3 groups. Lack of IκBα at this time point correlated well with initially unperturbed nuclear translocation of p65. However, starting at 30 min, a substantial increase in IκBα was seen in MK2- and HSP27-deficient cells compared with control cells. This increase reached the peak at 90 min and slowly decreased, but never returned to the control cell level over the next 3.5 h. Immunostaining of lung sections demonstrated a fourfold increase in IκBα protein (P = 6.7 × 10⁻⁵) in endothelial cells (as well as other lung cells) from immunized and challenged MK2 KO mice (Fig. 7 C). The expression of IκBα protein in lungs from nonimmunized control and KO mice was equal (unpublished data).

Increased IκBα mRNA in MK2–deficient cells upon TNFα stimulation

We studied the mechanism of increased expression of IκBα. MK2 and HSP27 were reported to impact the degradation of IκBα protein through the regulation of the IKK complex and proteasome (22, 23). Because the degradation of preexisting IκBα is intact in HSP27- and MK2-deficient cells, we studied the degradation of newly synthesized IκBα. We examined how quickly IκBα disappeared when protein synthesis was blocked by the addition of cycloheximide 80 min after TNFα-stimulation (Fig. 7 D). The rate of IκBα degradation in MK2- or HSP27-deficient cells was similar to that in control cells. Degradation of IκBα protein in cycloheximide-treated MK2- and HSP27-deficient cells was accompanied by the marked increase of nuclear NF-κB (Fig. 7 A). The activation of IKK was intact in MK2-deficient cells (Fig. 7 E).

Because we did not see decreased degradation of IκBα protein, we examined IκBα mRNA levels (Fig. 7 F). The rate at which IκBα mRNA increased upon addition of TNFα was much faster in MK2- or HSP27-deficient cells compared with control cells. For all three groups, IκBα mRNA peaked at 90 min. The peak of IκBα mRNA level (Fig. 7 E) was
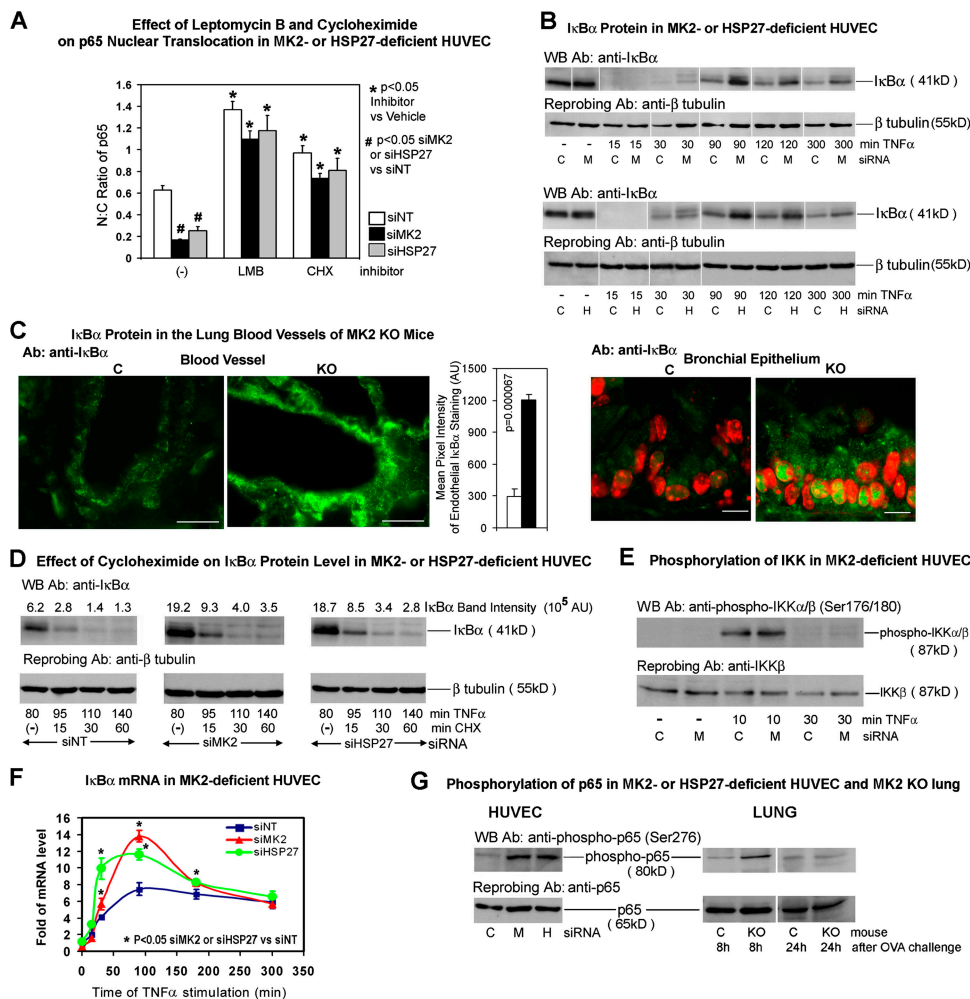
Figure 7.   The regulation of IκBα level by MK2 and HSP27. (A) After siRNA transfection (as in Fig. 6 A), HUVECs were preincubated with lepto-mycin B (LMB), cycloheximide (CHX), or vehicle (−), and then stimulated with TNFα for 3 h. Cells were then immunostained for p65. The p65 N:C ratio at 3 h of stimulation was measured as in Fig. 6 D ($n = 10$–20 representative cells from 3 separate experiments). (B) After siRNA trans-fection (as in Fig. 6 A), HUVECs were stimulated with TNFα for 15, 30, 90, 180, or 300 min, or they were left unstimulated (–). Cell lysates were Western blotted with anti–IκBα, followed by membrane reprobing with anti–β-tubulin antibody. C, control siNT; H, siHSP27; M, siMK2. (C) Lung sections from immunized and challenged mice (as in Fig. 1 A) were immuno-stained for IκBα (green) and treated with DAPI (nuclei pseudocolored in red). The two images to the left show IκBα staining in blood vessels. Bars, 10 μm. The two images to the right show IκBα and DAPI staining in the bronchial epithelium. Bars, 5 μm. The histogram shows mean pixel intensity (AU) of endothelial staining. Blood vessels of 0.1–1.5 mm lumen perimeter were examined ($n = 3$ mice per group). (D) HUVECs transfected as in Fig. 6 A were stimulated with TNFα. At 80 min of stimulation, cyclo-heximide (CHX) was added and cells were incubated for an additional

15, 30, or 60 min, and lysed. Control samples were lysed at 80 min of TNFα stimulation without CHX addition (−). Lysates were Western blotted with an anti-IκBα antibody. Membranes were reprobed with an anti-β-tubulin antibody. The IκBα band intensity was measured using Metamorph soft-ware and expressed in AUs. (E) After siRNA transfection (as in Fig. 6 A), HUVECs were stimulated with TNFα for 10 or 30 min or left unstimulated (−). Cell lysates were Western blotted with anti–phospho-IKKα/β (Ser 176/180 in IKKα and Ser 177/181 in IKKβ). The membrane was reprobed with anti-IKKβ antibody. C, control siNT; M, siMK2. (F) Cells transfected as in Fig. 6 A were stimulated as in Fig. 7 B. Real-time RT-PCR for IκBα and β-actin mRNA was performed. The quantity of IκBα mRNA was normal-ized to the quantity of β-actin mRNA. The results are expressed as the fold difference above the baseline quantity of normalized IκBα mRNA from siNT-transfected cells (set arbitrarily to 1; $n = 3$). (G) Cells trans-fected as in Fig. 6 A were stimulated with TNFα for 45 min (left). Lungs were obtained from mice 8 or 24 h after OVA challenge (right). Cell or lung lysates were Western blotted with an anti–phospho-p65 (Ser 276) antibody, followed by reprobing with anti-p65 antibody ($n = 3$). Error bars represent the SEM.

slightly delayed compared with the peak of nuclear p65 (Fig. 6 D). At 90 min, the IκBα mRNA concentration was 2 times higher in MK2-deficient cells and 1.6 times higher in HSP27-deficient cells than in control cells. After 90 min, the level of

IκBα mRNA rapidly decreased in MK2- or HSP27-deficient cells, but persisted at nearly the same level in control cells. This rapid drop in IκBα mRNA in MK2- or HSP27-deficient cells correlated well with the disappearance of p65 from the

nucleus. Therefore, there is a considerable elevation of IκBα mRNA at early time points after TNFα stimulation.

Increased phosphorylation of p65 at Ser 276 in MK2– and HSP27–deficient cells

Phosphorylation of p65 enhances its ability to recruit histone acetylases to NF-κB–driven promoter sites, and thereby enhances transcription (33). Phosphorylation of Ser276 is important for NF-κB–driven gene transcription in TNFα-stimulated cells (34). Western blotting demonstrated a significant increase

in Ser276 phosphorylation in MK2- and HSP27-deficent HUVECs 45 min after TNFα stimulation (Fig. 7 G, left). Phosphorylation of Ser276 was also transiently increased in the lungs of MK2 KO mice shortly after OVA challenge (Fig. 7 G, right).

Essential role of MSK1 in nuclear export of p65

We studied the kinases that are responsible for increased p65 phosphorylation. Ser276 is known to be targeted by two kinases: cytoplasmic PKAcα and nuclear MSK1 (35, 36).
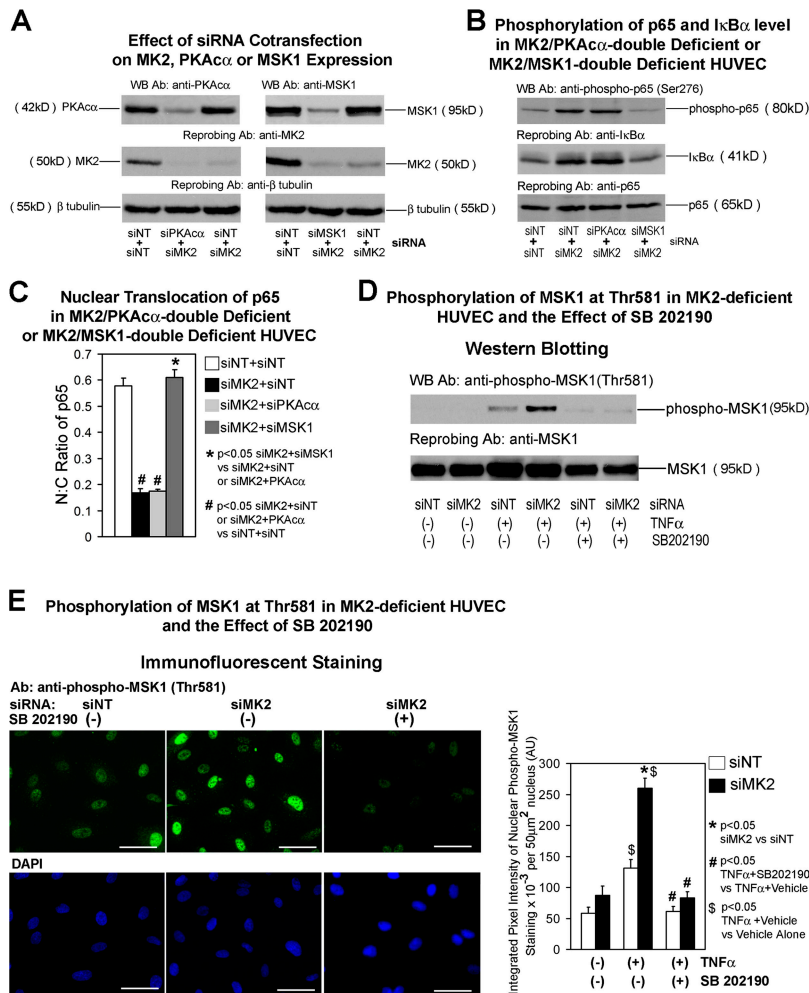

Figure 8.   The effect of MK2 on MSK1–driven nuclear export of p65. (A) HUVECs were cotransfected with siRNA against PKAcα (siPKAcα) and MK2 (siMK2; left) or MSK1 (siMSK1) and siMK2 (right). As a control, cells were cotransfected with siMK2 and nontargeting siRNA (siNT) or 2× siNT. Cell lysates were Western blotted with anti-PKAcα (top left) or anti-MSK1 (top right) antibodies. Membranes were reprobed sequentially with anti-MK2 antibody (middle) and with anti–β-tubulin antibodies (bottom; $n = 3$). (B) Cells cotransfected as in A were stimulated with TNFα for 45 min. Lysates were Western blotted with an anti–phospho-p65 (Ser 276) antibody (Ab), followed by sequential reprobing with an anti-IκBα and an anti-p65 antibodies. (C) Cells cotransfected as in A were stimulated with TNFα for 5 h and immunostained for p65 as in Fig. 6 B. The p65 N:C ratio was measured as in Fig. 6 D ($n = 20$–50 representative cells from 3 separate experiments). (D and E) HUVECs transfected with siRNA for MK2 or nontargeting siRNA (siNT) were preincubated with SB 202190 (SB 202190 +) or vehicle DMSO (SB 202190 −) and stimulated with TNFα for 30 min (TNFα +). Control cells were incubated with the vehicle without subsequent TNFα stimulation (TNFα −). (D) Cell lysates were Western blotted with an anti−phospho-MSK1 (Thr581) antibody and reprobed with an anti-MSK1 antibody. (E) Cells were stained with an anti−phospho-MSK1 (Thr581) antibody (green) and DAPI (blue). Bars, 25 μm. The histogram shows mean integrated intensity of phospho-MSK1 staining per 50 μm² nucleus ($n = 100$–200 representative cells from 3 separate experiments). Error bars represent the SEM.

HUVECs were cotransfected with two sets of siRNA; one targeting MK2 and one targeting PKAcα or MSK1 (Fig. 8 A). Cotransfection with MSK1 siRNA, but not PKAcα siRNA, inhibited p65 phosphorylation and brought the IκBα level to the control (nontargeting siRNA-transfected) cell level (Fig. 8 B). MSK1 knockdown, but not PKAcα knockdown, also reversed the shortened nuclear presence of p65 NF-κB (Fig. 8 C). Next, the impact of MK2 on MSK1 activation was examined (Fig. 8, D and E). Western blotting and immuno-staining with an anti–phospho–MSK1 (Thr581, activated form; [37]) revealed a pronounced increase in MSK1 activation in MK2-deficient HUVECs.
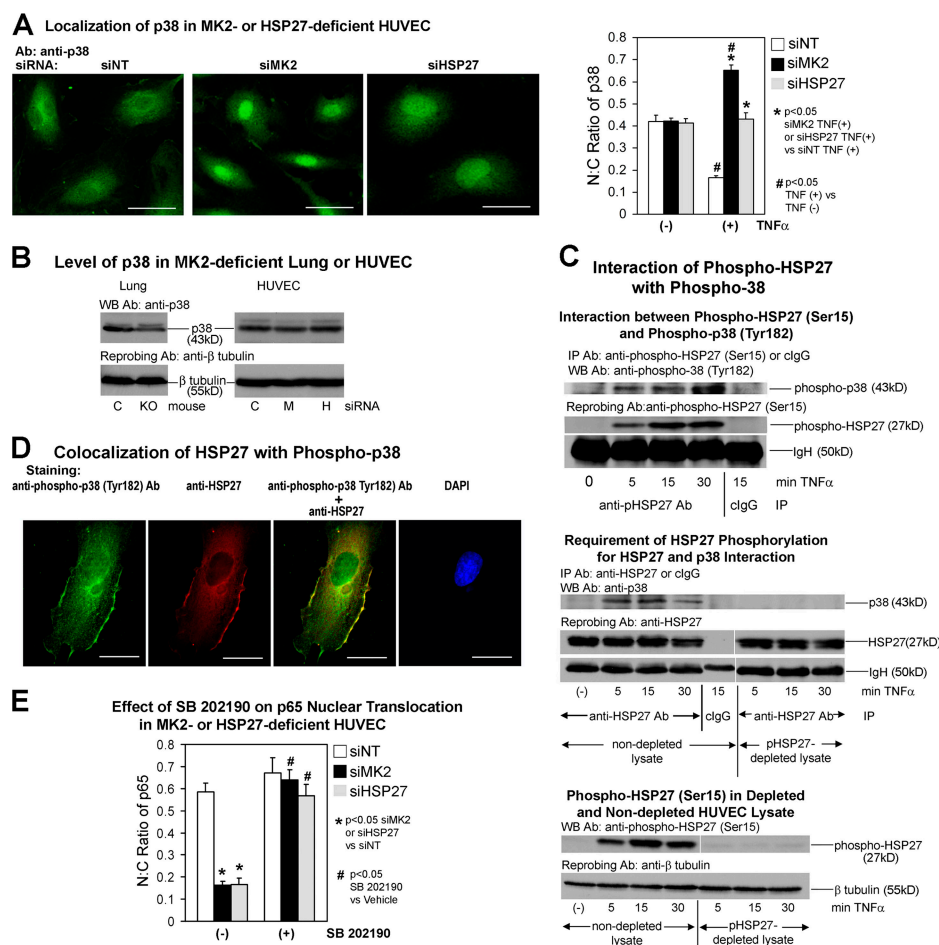

Figure 9. The effect of MK2 and HSP27 on nuclear localization of p38. (A) HUVECs transfected as in Fig. 6 A were stimulated with TNFα for 30 min (+) or left unstimulated (−). Cells were immunostained for p38 (green). Bars, 25 μm. The integrated intensity of cytoplasmic and nuclear p38 staining was measured. The histogram shows the N:C ratio of p38 staining (n = 30–50 representative cells from 3 separate experiments). (B) Lungs from immunized and challenged mice as in Fig. 1 A (left) or HUVECs transfected as in Fig. 6 A (right) were lysed, Western blotted with an anti-p38 antibody, and reprobed with an anti–β-tubulin antibody. (C, top) HUVECs were stimulated with TNFα for 5, 15, or 30 min or left unstimulated. Cells were lysed and immunoprecipitated with a rabbit anti–phospho-HSP27 (Ser15) antibody. An additional sample of stimulated cell lysate was immunoprecipitated with a control rabbit IgG (cIgG). Immunoprecipitates were Western blotted with anti–phospho-p38 (Tyr182), followed by reprobing with an anti–phospho-HSP27 (Ser15) antibody (n = 3). IgH, immunoglobulin heavy chain. (middle) An aliquot of a HUVEC lysate was depleted of phospho-HSP27 by two cycles of immunoprecipitation. The post-pHSP27 immuno-precipitation supernatant (pHSP27-depleted lysate) and another aliquot of the HUVEC lysate (nondepleted lysate) were then immuno-precipitated with an anti-HSP27 antibody. An isotype-specific mouse IgG (cIgG) was used as a control. Immunoprecipitates were Western blotted with an anti-p38 antibody, followed by reprobing with an anti-HSP27 antibody (n = 2). (bottom) An aliquot of a pHSP27-depleted lysate and a nondepleted HUVEC lysate were Western blotted with an anti–phospho-HSP27 (Ser15) antibody. The membrane was reprobed with an anti–β-tubulin antibody (n = 2). (D) HUVECs were stimulated with TNFα for 5, 15, and 30 min, immunostained for phospho-p38 (pTyr182, green) and HSP27 (red), and treated with DAPI (blue). Pictures show the cell after 15 min of stimulation (n = 2). Bar, 10 μm. Similar cytosolic colocalization of phospho-p38 and HSP27 was also seen after 5 and 30 min of stimulation (not depicted). (E) HUVECs were transfected as in Fig. 6 A, preincubated with SB 202190 (+) or vehicle (−), and stimulated with TNFα for 5 h. p65 immunostaining and N:C ratio measurement were performed as in Fig. 6, B and D, respectively (n = 10–20 representative cells from 3 experiments). Error bars represent the SEM.

Nuclear retention of p38 in MK2-deficient cells and reversal of shortened p65 nuclear presence by a p38 inhibitor

We examined the mechanism of increased MSK1 activation in MK2-deficient cells. p38 is known to activate MSK1 (38). Pretreatment of MK2 deficient HUVECs with the p38 inhibitor SB 202190 blocked TNFα-stimulated MSK1 phosphorylation (Fig. 8, D and E). MSK1 is found primarily in the nucleus (36). MK2 was reported to be essential for nuclear export of p38 upon cellular stress (39). This process required direct interaction between MK2 and p38. We investigated the cellular distribution of p38. Immunostaining showed that p38 redistributed from the nucleus to cytoplasm upon TNFα stimulation in control cells, as previously reported (39), but accumulated in the nucleus of MK2- and HSP27-deficient cells (Fig. 9 A). We believe that retention of p38 in the nucleus in the absence of MK2 leads to phosphorylation and activation of its nuclear substrate MSK1. MK2 was reported to regulate the level of p38 protein (40). We detected a minor decrease in p38 level in the lungs of MK2 KO mice (Fig. 9 B). The expression of p38 was not decreased in MK2- or HSP27-deficient HUVECs. Our results are in agreement with the previously cited paper (40), which showed that the regulation of p38 level by MK2 is cell specific. Next, we addressed the mechanism of nuclear accumulation of p38 in HSP27-deficient cells. Phospho-HSP27 (Ser15) coprecipitated with phospho-p38 in TNFα-stimulated cells (Fig. 9 C, top). HSP27 lacking phosphorylation at Ser15 did not interact with p38 (Fig. 9 C, middle and bottom). Phospho-p38 and HSP27 strongly colocalized in the cytoplasm, but not in the nucleus, in the course of TNFα stimulation (5, 15, and 30 min). Colocalization at the 15-min time point is shown in Fig. 9 D. The results suggest that phospho-HSP27 binds to cytoplasmic phospho-p38 and blocks its translocation to the nucleus. Next, we studied the role of p38 in nuclear retention of p65. Inhibition of p38 with SB 202190 reversed the shortened nuclear presence of NF-κB in MK2- and HSP27- deficient cells (Fig. 9 E).

Decreased stress fiber formation reduced VCAM-1, but not ICAM-1, expression as a consequence of MK2 or HSP27 deficiency

We studied if the MK2–HSP27 pathway directly controlled endothelial cell function. MK2- and HSP27-deficient cells showed 2.9- and 3.7-fold reduction in actin polymerization, respectively (P < 0.05 for both cell types; Fig. 10 A). HSP27-deficient cells demonstrated almost complete inhibition of TNFα-stimulated VCAM-1 expression (Fig. 10 B, top graph; P = 5.5×10^{-4}). ICAM-1 expression was not affected by HSP27 deficiency (Fig. 10 B, bottom graph).

Temporal control of NF-κB–induced transcript levels by MK2

We examined if the expression of other NF-κB–inducible genes was directly controlled by the MK2 pathway (Fig. 10 C). NF-κB–inducible genes can be classified into two groups: early-phase genes (e.g., IL-6 and Rel) and sustained-phase genes (early and late; e.g., E selectin and MCP-1). We have already shown that the expression of the early-phase target IκBα and the sustained-phase target VCAM-1 is increased and decreased, respectively, in MK2 KO mice. In agreement, MK2-deficient HUVECs showed a substantial increase in IL-6 and Rel transcripts, but a marked decrease in E selectin and MCP-1 transcripts. The decrease in E-selectin and MCP-1 is likely to be important because both contribute to leukocyte extravasation and inflammation.

Reduced adhesion and transendothelial migration of mononuclear cells (MNCs) through a HSP27-deficient HUVEC monolayer

We studied adhesion and transendothelial migration of normal peripheral blood MNCs through TNFα-activated, HSP27-deficient HUVECs. The percentage of MNCs that adhered to HSP27-sufficient and –deficient cells was 35.3 ± 0.3% and 18.5 ± 0.6%, respectively (P = 7.9×10^{-6}; Fig. 10 D, left graph). MNC migration under the gradient of MCP-1 through the HSP27-deficient cell monolayer was severely reduced (P = 0.0036) compared with migration through control cell monolayer (Fig. 10 D, right graph). We believe that the impaired actin polymerization and adhesion molecule expression caused by HSP27 deficiency results in the failure of MNCs to adhere to and migrate through the endothelial cell monolayer.

DISCUSSION

We have identified MK2–HSP27 as a critical signaling pathway regulating endothelial barrier and inflammation. MK2 KO mice are unable to mount an airway allergic inflammation. MK2 deficiency does not impair systemic Th2 response, but results in reduced endothelial permeability. The decreased permeability correlates with the impaired actin polymerization and lack of adherens junction disruption. In the absence of MK2, the expression of critical adhesion molecules and chemokines is impaired. Thus, MK2 regulates the development of the local (lung) inflammation primarily by controlling endothelium.

MK2 seems to regulate select genes, cells, and organs. OVA-sensitized MK2 KO mice demonstrate decreased expression of Th2 cytokines in the lung, but normal production of innate, Th1, and Th2 cytokines in the liver. It has been previously shown that MK2 KO mice clear *Listeria monocytogenes* from the liver and blood, but not from the lung (41). MK2 KO mice have a defect in the synthesis of TNF-α and IFN-γ. The production of IL-1 and -6 is decreased in spleen cells (9), but not in bone marrow–derived macrophages (41). The results suggest a heterogeneous response that is perhaps caused by different disease models that have been examined. The heterogeneous response also likely results from the variable expression pattern of MK2 and HSP27 in different organs and cells.

VCAM-1, but not ICAM-1, expression is regulated by the p38 pathway (6). NF-κB is a major transcription factor for VCAM-1 (20). MK2 is essential for sustained nuclear presence of NF-κB (Fig. 10 E). MK2 prevents premature export of NF-κB from the nucleus by decreasing the NF-κB–driven
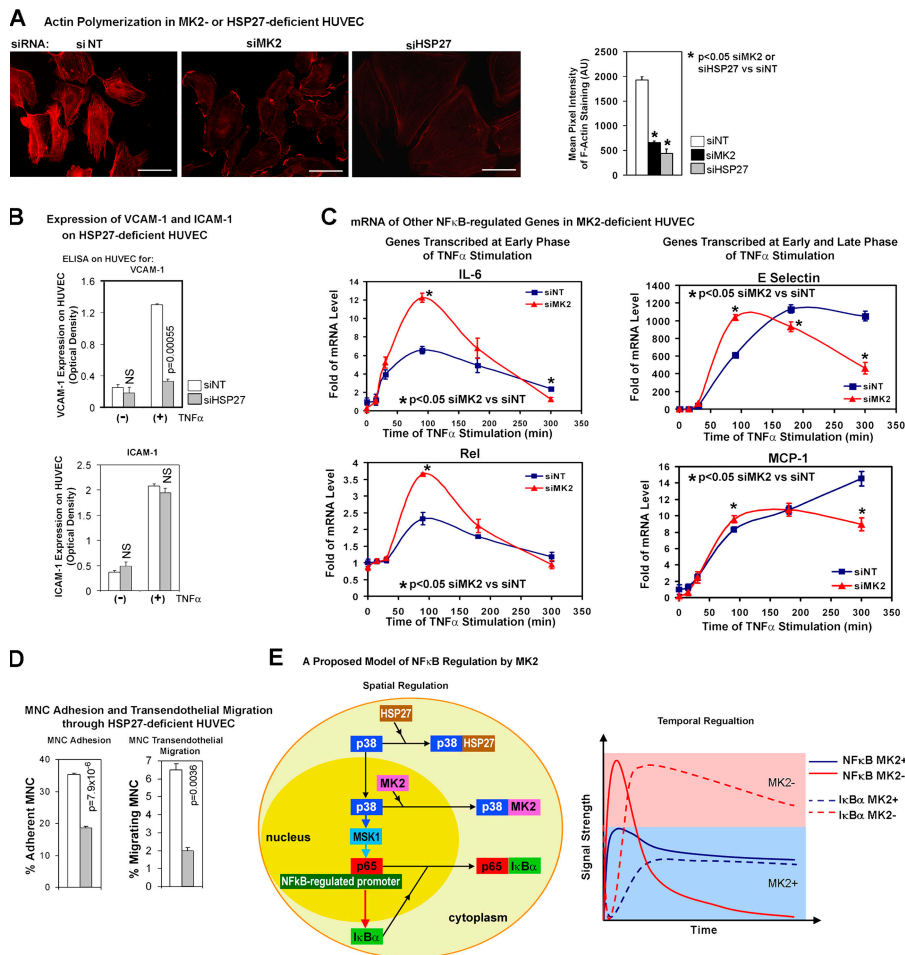
Figure 10. Direct effect of MK2 and HSP27 on endothelial cell function. (A) HUVECs were transfected as in Fig. 6 A, stimulated with TNFα for 30 min and stained with rhodamine-labeled phalloidin to detect polymerized actin (red). Bars, 50 μm. The histogram shows mean pixel intensity of staining per cell ($n = 20$–30 representative cells from 3 experiments). Staining intensity is expressed in AU. (B) HUVECs transfected with siHSP27 and siNT as in Fig. 6 A were assayed for VCAM-1 (top histogram) or ICAM-1 (bottom histogram) expression by ELISA. Histograms show mean optical density at 450 nm as a measure of VCAM-1 (left) or ICAM-1 (right) expression per well (each experiment in triplicates, $n = 3$). (C) Kinetics of NF-κB target gene mRNA expression in MK2-deficient HUVECs after TNFα stimulation was assessed. Cells transfected with siMK2 or siNT as in Fig. 6 A were stimulated as in Fig. 7 E. mRNA for IL-6, Rel, E selectin, MCP-1, and β-actin was measured by real-time RT-PCR. The quantity of IL-6, Rel, E-selectin, and MCP-1 mRNA was normalized to the quantity of β-actin mRNA. Results are expressed as fold difference above the baseline quantity of normalized mRNA from siNT-transfected cells (set arbitrarily to 1; $n = 3$). (D) HUVECs were transfected as in Fig. 10 B. The adhesion of human peripheral blood MNCs to transfected TNFα-treated HUVECs and the migration of MNCs through the transfected and TNFα-treated HUVEC monolayer in transwells were measured. The mean percentage of MNCs that adhered to (left) or migrated (right)

through the HUVEC layer is shown (each experiment in triplicates; $n = 3$). (E) A proposed model of NF-κB regulation by MK2. (left) Spatial regulation of NF-κB by the MK2 pathway. Phospho-HSP27 binds p38 in the cytoplasm and prevents its translocation to the nucleus. MK2 facilitates export of p38 from the nucleus. By reducing the level of p38 in the nucleus, MK2 and HSP27 decrease the phosphorylation of nuclear MSK1. This results in reduced p65 phosphorylation and IκBα expression. Newly synthesized IκBα mediates nuclear export of p65 and functions as a negative feedback for the NF-κB pathway. By regulating p38 and MSK1, the MK2 pathway controls the level of the negative feedback in the NF-κB pathway (black arrow, translocation; colored arrow, enzymatic or transcriptional effect). (right) Temporal regulation of NF-κB signal strength by the MK2 pathway. In the presence of MK2 in normal cells (MK2+), the initial burst of NF-κB causes a modest increase in IκBα synthesis, which results in a tempered export of NF-κB and its prolonged transcriptional activity. In the absence of MK2 (MK2−, pink zone), the NF-κB signal strength overshoots in the early phase because of enhanced p65 phosphorylation. This causes an overzealous IκBα response, leading to premature export of NF-κB. As a result, the late-phase transcriptional activity of NF-κB is lost. MK2 switches the pattern of NF-κB activation from elevated, but short lasting, to moderate-level, but prolonged. Error bars represent the SEM.

transcription of its exporter IκBα. MK2 reduces the level of p65 NF-κB phosphorylation. The latter occurs through the sequential action of p38 and MSK1. Under normal circumstances, MK2 facilitates export of p38 from the nucleus (39), and thereby adjusts the magnitude of negative feedback in the NF-κB pathway. MK2 decreases the amplitude of the early-phase NF-κB signal and converts it into a sustained phase signal. Thus, we provide a novel mechanism for a regulatory cross-talk between the p38 and NF-κB pathways through MK2 and MSK1. We also uncovered a mechanism for cytoplasmic retention of p38 through the physical interaction with phospho-HSP27. The subcellular distribution of p38 is regulated by its two downstream molecules. MK2 exports p38 from the nucleus and HSP27 retains it in the cytosol.

Previously, Park et al. linked the p38 MAPK–MSK1/2 pathway to a subset of NF-κB target genes in macrophages through two different mechanisms—one through the phosphorylation of CREB (Ser133) and the other through chromatin modification (42). In our study, the phosphorylation of CREB (Ser133) was unchanged in MK2 KO mice compared with control mice. Thus, CREB is unlikely to explain the phenotype of the MK2 KO mice. We did not examine the effect of the MK2 knockout on chromatin modification of NF-κB target genes. Thus, it is possible that additional mechanisms contribute to the phenotype that was observed in MK2 KO mice. In summary, we have identified a critical role for MK2 and HSP27 in endothelial cell signaling. MK2 and HSP27 regulate aspects of endothelial function that are essential for their permeability and adhesiveness to inflammatory cells. Inability to regulate this endothelial function leads to an aborted local immune response in the face of a normal systemic immune response. Thus, MK2 and HSP27 represent attractive targets for therapeutic intervention in asthma and other inflammatory diseases.

MATERIALS AND METHODS

Mice. MK2 knockout C57BL/6J mice were generated in Dr. Matthias Gaestel's laboratory (9). All procedures on mice were approved by the University of Texas Medical Branch and the National Jewish Medical and Research Center Institutional Animal Care and Use Committees and performed according to committee guidelines.

Immunization, inhalation challenge, BAL, and endothelial permeability. OVA sensitization, inhalation challenge, and BAL of mice were done as previously described (10). The intranasal administration of LPS or saline (control) was done as previously described (43). Mice were killed 8 h after LPS or saline administration. Lung vascular permeability was measured as previously described (11).

Measurement of AHR. Anesthetized mice were connected to a ventilator (FlexiVent; SCIREQ) via a tracheal 18-gauge cannula and ventilated under constant flow conditions limited to 30 cm H_2O at a frequency of 150 breaths/min with a tidal volume of 8 ml/kg, while breathing against an artificial positive end-expiratory pressure of 2.5 cm H_2O. Before the measurements were taken, lungs were inflated four times to total lung capacity. For resistance measurements, a single-frequency (2.5-Hz) sinusoidal piston volume movement with a peak tidal volume of 0.15 ml was applied. Pressure, volume, and flow data were fit to the linear single compartment model to obtain values for total lung resistance. A baseline lung resistance (no aerosol administration), lung resistance in response to saline alone, and lung resistance to increasing doses of methacholine (6.25–50 mg/ml in saline) aerosol

were sequentially obtained. Airway resistance was measured several times at each methacholine dose, and three peak resistance values (coherence >90%) were taken into account.

Adoptive transfer of OT-2 T cells. Adoptive transfer of activated OT-2 T cells to MK2 KO and control mice and the exposure of transferred animals to OVA aerosol were performed according to the previously described protocol (16).

Histology, immunofluorescent staining, and phalloidin staining of filamentous actin. Hematoxylin and eosin (HE), periodic acid-Schiff (PAS), and Trichrome staining of lung sections was done at the University of Texas Medical Branch or National Jewish Medical and Research Center Histology Core Laboratories according to the standard protocol. Immunofluorescent staining of lung sections and paraformaldehyde-fixed HUVECs were performed as previously described (44). For actin staining, samples were permeabilized with 0.05% saponin in PBS for 15 min and incubated with rhodamine-labeled phalloidin (Sigma-Aldrich) at 0.2 μg/ml for 30 min

ELISA to measure the DNA-binding capacity of NF-κB p65. The ability of NF-κB p65 from the nuclear extract to bind the DNA consensus sequence was assessed using an ELISA-based TransAM NF-κB p65 kit (Active Motif, Inc.) according to the manufacturer's protocol.

Real-time PCR. RNA purified from Trizol (Invitrogen) lysates was reverse transcribed using Superscript III (Invitrogen) according to the manufacturer protocol. SYBR Green PCR Master Mix (Applied Biosystems) was used for DNA amplification. Primer sequences are shown in the Supplemental materials and methods (available at http://www.jem.org/cgi/content/full/jem .20062621/DC1). Real-time PCR was performed with the ABI Prism 7000 Sequence Detection System (Applied Biosystems).

OVA-specific IgE, cytokine production, and splenocyte proliferation. The ELISA for OVA-specific IgE was performed as previously described (10). IL-4, IL-5, IFNγ, and TNFα in liver lysates was quantified by ELISA according to the manufacturer's protocol (OptEIA sets; BD Biosciences) and adjusted for the protein concentration. Thymidine incorporation assay was performed as previously described (45).

Chemotaxis assays. CD4 T cell chemotaxis to 10^{-7} M MCP-1 was performed as previously described (46). CD4 T cells were isolated from the splenocyte suspension by negative selection using a CD4 T Cell Isolation kit (Miltenyi Biotec). The transendothelial migration assay was performed as previously described (47). Peripheral blood MNC migration through the TNFα-stimulated HUVEC monolayer was induced by MCP-1 at 10^{-7} M.

HUVEC culture and stimulation. HUVECs (Clonetics; passage 1–4) were cultured in EGM-2 media (Clonetics) as recommended by the manufacturer. For Western blotting, real-time PCR and immunofluorescent staining experiment HUVECs were stimulated with TNFα at 10 ng/ml. When indicated, cycloheximide, leptomycin B, or SB 202190 was added 30 min before TNFα stimulation at 25 μg/ml, 20 nM, and 1 μg/ml, respectively.

Transfection of HUVECs with siRNA or plasmids. siRNA oligonucleotide sequence for human HSP27 and human MK2 were previously described (22, 48). siRNA for PKAcα and for MSK1 were obtained from the predesigned siGenome collection from Dharmacon. As a negative control, siRNA against firefly luciferase (siControl Non-Targeting siRNA # 2; Dharmacon) was used. HA-tagged human HSP27 WT and HSP27 Ser78, 82Ala mutant in pcDNA3 expression vector were a gift from M. Gaestel (Hannover Medical School, Hannover, Germany). Mutation of Ser15 to Ala (AGC to GCC) in HSP27 Ser78, 82Ala cDNA-containing vector was performed using the QuikChange (Stratagene) site-directed mutagenesis protocol, as previously described (45). HUVEC transfection was performed as previously described (49).

HUVEC lysis, immunoprecipitation, electrophoresis, and Western blotting. Preparation of HUVEC lysate in the modified RIPA buffer, immunoprecipitation, and Western blotting were performed as previously described (45).

VCAM-1 and ICAM-1 ELISA and adhesion assay with HUVECs. VCAM-1 and ICAM-1 expression on HUVECs was measured by ELISA, as previously described (50). For the adhesion assay, CMTMR-labeled MNCs (2×10^5) were added to washed HUVEC monolayers and incubated at $37°C$ in 5% CO_2 for 1 h. After washing, adherent cells were recovered by trypsinization and CMTMR-positive cells were counted.

Morphometric and statistical analysis. For quantification of fluorescence and light microscopic results, data from 2–10 fields per lung section obtained from 3–8 mice per group were analyzed. For morphometric analyses, we studied mid-size bronchi of the epithelial basement membrane (BM) perimeter in the range of 0.4–2.0 mm (51–53). The results are expressed as a staining-positive area or the number of staining-positive (e.g., PAS) cells per unit (1 mm) of the BM perimeter. To measure inflammation (HE staining) or ECM deposition (Trichrome staining), the areas of peribronchial cellular infiltrate or peribronchial areas positive for blue color, respectively, were traced and circled using the region selection tool of the morphometric software (MetaMorph; Invitrogen) as previously described (54, 55). Individual areas of inflammation or ECM deposition around a single bronchus were added and the area sum was divided by the BM perimeter. To assess mucus production, the number of purple stain–positive cells (PAS staining) in the epithelium of mid-size bronchi was counted as previously described (55). For blood vessel studies, we examined small to mid-size blood vessels of 0.1–1.5-mm lumen perimeter. The fluorescent microscopy image analysis was as follows. Integrated pixel intensity was defined as a sum of fluorescent intensities of all pixels in the measured area. Mean pixel intensity was defined as integrated intensity divided by the measured area. The same exposure time was used to capture images in all experimental groups in a particular set of experiments. Fluorescent staining-positive areas were defined using the intensity threshold command. The same threshold was applied to all images from a particular set of experiments. Statistical analysis was done by two-tailed Student's t test. Results are shown as the mean $\pm$ the SEM. $P < 0.05$ was considered statistically significant.

Online supplemental material. Fig. S1 shows images of polymerized actin in the pulmonary endothelium from MK2 KO and control mice at different time points after OVA challenge. Fig. S2 shows airway remodeling (PAS, Trichrome staining, and immunostaining for smooth muscle actin) of MK2 KO and control mice. Supplemental material and methods contain the list of antibodies and sequences of real-time PCR primers. The online version of this article is available at http://www.jem.org/cgi/content/full/jem.20062621/DC1.

REFERENCES

1. Liu, Y., S.K. Shaw, S. Ma, L. Yang, F.W. Luscinskas, and C.A. Parkos. 2004. Regulation of leukocyte transmigration: cell surface interactions and signaling events. *J. Immunol.* 172:7–13.
2. Nakajima, H., H. Sano, T. Nishimura, S. Yoshida, and I. Iwamoto. 1994. Role of vascular cell adhesion molecule 1/very late activation antigen 4 and intercellular adhesion molecule 1/lymphocyte function–associated antigen 1 interactions in antigen-induced eosinophil and T cell recruitment into the tissue. *J. Exp. Med.* 179:1145–1154.
3. Del Maschio, A., A. Zanetti, M. Corada, Y. Rival, L. Ruco, M.G. Lampugnani, and E. Dejana. 1996. Polymorphonuclear leukocyte adhesion triggers the disorganization of endothelial cell-to-cell adherens junctions. *J. Cell Biol.* 135:497–510.
4. Stamatovic, S.M., R.F. Keep, S.L. Kunkel, and A.V. Andjelkovic. 2003. Potential role of MCP-1 in endothelial cell tight junction 'opening': signaling via Rho and Rho kinase. *J. Cell Sci.* 116:4615–4628.
5. Wang, Q., M. Yerukhimovich, W.A. Gaarde, I.J. Popoff, and C.M. Doerschuk. 2005. MKK3 and -6-dependent activation of p38alpha MAP kinase is required for cytoskeletal changes in pulmonary microvascular endothelial cells induced by ICAM-1 ligation. *Am. J. Physiol. Lung Cell Mol. Physiol.* 288:L359–L369.
6. Pietersma, A., B.C. Tilly, M. Gaestel, N. de Jong, J.C. Lee, J.F. Koster, and W. Sluiter. 1997. p38 mitogen activated protein kinase regulates endothelial VCAM-1 expression at the post-transcriptional level. *Biochem. Biophys. Res. Commun.* 230:44–48.
7. Goebeler, M., K. Kilian, R. Gillitzer, M. Kunz, T. Yoshimura, E.B. Brocker, U.R. Rapp, and S. Ludwig. 1999. The MKK6/p38 stress kinase cascade is critical for tumor necrosis factor-alpha-induced expression of monocyte-chemoattractant protein-1 in endothelial cells. *Blood.* 93:857–865.
8. Ben-Levy, R., I.A. Leighton, Y.N. Doza, P. Attwood, N. Morrice, C.J. Marshall, and P. Cohen. 1995. Identification of novel phosphorylation sites required for activation of MAPKAP kinase-2. *EMBO J.* 14:5920–5930.
9. Kotlyarov, A., A. Neininger, C. Schubert, R. Eckert, C. Birchmeier, H.D. Volk, and M. Gaestel. 1999. MAPKAP kinase 2 is essential for LPS-induced TNF-alpha biosynthesis. *Nat. Cell Biol.* 1:94–97.
10. Stafford, S., H. Li, P.A. Forsythe, M. Ryan, R. Bravo, and R. Alam. 1997. Monocyte chemotactic protein-3 (MCP-3)/fibroblast-induced cytokine (FIC) in eosinophilic inflammation of the airways and the inhibitory effects of an anti-MCP-3/FIC antibody. *J. Immunol.* 158:4953–4960.
11. Lee, K.S., S.R. Kim, H.S. Park, G.Y. Jin, and Y.C. Lee. 2004. Cysteinyl leukotriene receptor antagonist regulates vascular permeability by reducing vascular endothelial growth factor expression. *J. Allergy Clin. Immunol.* 114:1093–1099.
12. Kayyali, U.S., C.M. Pennella, C. Trujillo, O. Villa, M. Gaestel, and P.M. Hassoun. 2002. Cytoskeletal changes in hypoxic pulmonary endothelial cells are dependent on MAPK-activated protein kinase MK2. *J. Biol. Chem.* 277:42596–42602.
13. Cattelino, A., S. Liebner, R. Gallini, A. Zanetti, G. Balconi, A. Corsi, P. Bianco, H. Wolburg, R. Moore, B. Oreda, et al. 2003. The conditional inactivation of the β-catenin gene in endothelial cells causes a defective vascular pattern and increased vascular fragility. *J. Cell Biol.* 162:1111–1122.
14. Nadel, J.A., and P.R. Burgel. 2001. The role of epidermal growth factor in mucus production. *Curr. Opin. Pharmacol.* 1:254–258.
15. Burgel, P.R., S.C. Lazarus, D.C. Tam, I.F. Ueki, K. Atabai, M. Birch, and J.A. Nadel. 2001. Human eosinophils induce mucin production in airway epithelial cells via epidermal growth factor receptor activation. *J. Immunol.* 167:5948–5954.
16. Beier, K.C., A. Hutloff, M. Lohning, T. Kallinich, R.A. Kroczek, and E. Hamelmann. 2004. Inducible costimulator-positive T cells are required for allergen-induced local B-cell infiltration and antigen-specific IgE production in lung tissue. *J. Allergy Clin. Immunol.* 114:775–782.
17. Lukacs, N.W. 2001. Role of chemokines in the pathogenesis of asthma. *Nature Rev. Immunol.* 1:108–116.
18. Chaplin, D.D. 2002. Cell cooperation in development of eosinophil-predominant inflammation in airways. *Immunol. Res.* 26:55–62.
19. Hosking, B.M., S.C. Wang, M. Downes, P. Koopman, and G.E. Muscat. 2004. The VCAM-1 gene that encodes the vascular cell adhesion molecule is a target of the Sry-related high mobility group box gene, Sox18. *J. Biol. Chem.* 279:5314–5322.
20. Neish, A.S., A.J. Williams, H.J. Palmer, M.Z. Whitley, and T. Collins. 1992. Functional analysis of the human vascular cell adhesion molecule 1 promoter. *J. Exp. Med.* 176:1583–1593.
21. Ozes, O.N., L.D. Mayo, J.A. Gustin, S.R. Pfeffer, L.M. Pfeffer, and D.B. Donner. 1999. NF-kappaB activation by tumour necrosis factor requires the Akt serine-threonine kinase. *Nature.* 401:82–85.

22. Park, K.J., R.B. Gaynor, and Y.T. Kwak. 2003. Heat shock protein 27 association with the I kappa B kinase complex regulates tumor necrosis factor alpha-induced NF-kappa B activation. *J. Biol. Chem.* 278:35272–35278.

23. Parcellier, A., E. Schmitt, S. Gurbuxani, D. Seigneurin-Berny, A. Pance, A. Chantome, S. Plenchette, S. Khochbin, E. Solary, and C. Garrido. 2003. HSP27 is a ubiquitin-binding protein involved in I-kappa-Balpha proteasomal degradation. *Mol. Cell. Biol.* 23:5790–5802.

24. Benndorf, R., K. Hayess, S. Ryazantsev, M. Wieske, J. Behlke, and G. Lutsch. 1994. Phosphorylation and supramolecular organization of murine small heat shock protein HSP25 abolish its actin polymerization-inhibiting activity. *J. Biol. Chem.* 269:20780–20784.

25. Doppler, H., P. Storz, J. Li, M.J. Comb, and A. Toker. 2005. A phosphorylation state-specific antibody recognizes Hsp27, a novel substrate of protein kinase D. *J. Biol. Chem.* 280:15013–15019.

26. Steinbrecher, K.A., W. Wilson III, P.C. Cogswell, and A.S. Baldwin. 2005. Glycogen synthase kinase 3beta functions to specify gene-specific, NF-kappaB-dependent transcription. *Mol. Cell. Biol.* 25:8444–8455.

27. Chen, G., M.S. Bhojani, A.C. Heaford, D.C. Chang, B. Laxman, D.G. Thomas, L.B. Griffin, J. Yu, J.M. Coppola, T.J. Giordano, et al. 2005. Phosphorylated FADD induces NF-kappaB, perturbs cell cycle, and is associated with poor outcome in lung adenocarcinomas. *Proc. Natl. Acad. Sci. USA.* 102:12507–12512.

28. Legembre, P., B.C. Barnhart, L. Zheng, S. Vijayan, S.E. Straus, J. Puck, J.K. Dale, M. Lenardo, and M.E. Peter. 2004. Induction of apoptosis and activation of NF-kappaB by CD95 require different signalling thresholds. *EMBO Rep.* 5:1084–1089.

29. Stokoe, D., K. Engel, D.G. Campbell, P. Cohen, and M. Gaestel. 1992. Identification of MAPKAP kinase 2 as a major enzyme responsible for the phosphorylation of the small mammalian heat shock proteins. *FEBS Lett.* 313:307–313.

30. Johnson, C., D. Van Antwerp, and T.J. Hope. 1999. An N-terminal nuclear export signal is required for the nucleocytoplasmic shuttling of IkappaBalpha. *EMBO J.* 18:6682–6693.

31. Arenzana-Seisdedos, F., P. Turpin, M. Rodriguez, D. Thomas, R.T. Hay, J.L. Virelizier, and C. Dargemont. 1997. Nuclear localization of I kappa B alpha promotes active transport of NF-kappa B from the nucleus to the cytoplasm. *J. Cell Sci.* 110(Pt 3):369–378.

32. Klement, J.F., N.R. Rice, B.D. Car, S.J. Abbondanzo, G.D. Powers, P.H. Bhatt, C.H. Chen, C.A. Rosen, and C.L. Stewart. 1996. IkappaBalpha deficiency results in a sustained NF-kappaB response and severe widespread dermatitis in mice. *Mol. Cell. Biol.* 16:2341–2349.

33. Zhong, H., R.E. Voll, and S. Ghosh. 1998. Phosphorylation of NF-kappa B p65 by PKA stimulates transcriptional activity by promoting a novel bivalent interaction with the coactivator CBP/p300. *Mol. Cell.* 1:661–671.

34. Okazaki, T., S. Sakon, T. Sasazuki, H. Sakurai, T. Doi, H. Yagita, K. Okumura, and H. Nakano. 2003. Phosphorylation of serine 276 is essential for p65 NF-kappaB subunit-dependent cellular responses. *Biochem. Biophys. Res. Commun.* 300:807–812.

35. Zhong, H., H. Suyang, H. Erdjument-Bromage, P. Tempst, and S. Ghosh. 1997. The transcriptional activity of NF-kappaB is regulated by the IkappaB-associated PKAc subunit through a cyclic AMP-independent mechanism. *Cell.* 89:413–424.

36. Vermeulen, L., G. De Wilde, P. Van Damme, W. Vanden Berghe, and G. Haegeman. 2003. Transcriptional activation of the NF-kappaB p65 subunit by mitogen- and stress-activated protein kinase-1 (MSK1). *EMBO J.* 22:1313–1324.

37. McCoy, C.E., D.G. Campbell, M. Deak, G.B. Bloomberg, and J.S. Arthur. 2005. MSK1 activity is controlled by multiple phosphorylation sites. *Biochem. J.* 387:507–517.

38. Deak, M., A.D. Clifton, L.M. Lucocq, and D.R. Alessi. 1998. Mitogen- and stress-activated protein kinase-1 (MSK1) is directly activated by MAPK and SAPK2/p38, and may mediate activation of CREB. *EMBO J.* 17:4426–4441.

39. Ben-Levy, R., S. Hooper, R. Wilson, H.F. Paterson, and C.J. Marshall. 1998. Nuclear export of the stress-activated protein kinase p38 mediated by its substrate MAPKAP kinase-2. *Curr. Biol.* 8:1049–1057.

40. Kotlyarov, A., Y. Yannoni, S. Fritz, K. Laass, J.B. Telliez, D. Pitman, L.L. Lin, and M. Gaestel. 2002. Distinct cellular functions of MK2. *Mol. Cell. Biol.* 22:4827–4835.

41. Lehner, M.D., F. Schwoebel, A. Kotlyarov, M. Leist, M. Gaestel, and T. Hartung. 2002. Mitogen-activated protein kinase-activated protein kinase 2-deficient mice show increased susceptibility to Listeria monocytogenes infection. *J. Immunol.* 168:4667–4673.

42. Park, J.M., F.R. Greten, A. Wong, R.J. Westrick, J.S.C. Arthur, K. Otsu, A. Hoffmann, M. Montminy, and M. Karin. 2005. Signaling pathways and genes that inhibit pathogen-induced macrophage apoptosis—CREB and NF-κB as key regulators. *Immunity.* 23:319–329.

43. Poynter, M.E., C.G. Irvin, and Y.M. Janssen-Heininger. 2003. A prominent role for airway epithelial NF-kappa B activation in lipopolysaccharide-induced airway inflammation. *J. Immunol.* 170:6257–6265.

44. Gorska, M.M., O. Cen, Q. Liang, S.J. Stafford, and R. Alam. 2006. Differential regulation of interleukin 5-stimulated signaling pathways by dynamin. *J. Biol. Chem.* 281:14429–14439.

45. Gorska, M.M., S.J. Stafford, O. Cen, S. Sur, and R. Alam. 2004. Unc119, a novel activator of Lck/Fyn, is essential for T cell activation. *J. Exp. Med.* 199:369–379.

46. Fong, A.M., R.T. Premont, R.M. Richardson, Y.R. Yu, R.J. Lefkowitz, and D.D. Patel. 2002. Defective lymphocyte chemotaxis in beta-arrestin2- and GRK6-deficient mice. *Proc. Natl. Acad. Sci. USA.* 99:7478–7483.

47. Mohan, K., Z. Ding, J. Hanly, and T.B. Issekutz. 2002. IFN-gamma-inducible T cell alpha chemoattractant is a potent stimulator of normal human blood T lymphocyte transendothelial migration: differential regulation by IFN-gamma and TNF-alpha. *J. Immunol.* 168:6420–6428.

48. Manke, I.A., A. Nguyen, D. Lim, M.Q. Stewart, A.E. Elia, and M.B. Yaffe. 2005. MAPKAP kinase-2 is a cell cycle checkpoint kinase that regulates the G2/M transition and S phase progression in response to UV irradiation. *Mol. Cell.* 17:37–48.

49. Nishiwaki, Y., T. Yokota, M. Hiraoka, M. Miyagishi, K. Taira, M. Isobe, H. Mizusawa, and M. Yoshida. 2003. Introduction of short interfering RNA to silence endogenous E-selectin in vascular endothelium leads to successful inhibition of leukocyte adhesion. *Biochem. Biophys. Res. Commun.* 310:1062–1066.

50. Nagata, M., J.B. Sedgwick, R. Vrtis, and W.W. Busse. 1999. Endothelial cells upregulate eosinophil superoxide generation via VCAM-1 expression. *Clin. Exp. Allergy.* 29:550–561.

51. Wiggs, B.R., C. Bosken, P.D. Pare, A. James, and J.C. Hogg. 1992. A model of airway narrowing in asthma and in chronic obstructive pulmonary disease. *Am. Rev. Respir. Dis.* 145:1251–1258.

52. Hamid, Q., Y. Song, T.C. Kotsimbos, E. Minshall, T.R. Bai, R.G. Hegele, and J.C. Hogg. 1997. Inflammation of small airways in asthma. *J. Allergy Clin. Immunol.* 100:44–51.

53. Kotsimbos, A.T., M. Humbert, E. Minshall, S. Durham, R. Pfister, G. Menz, J. Tavernier, A.B. Kay, and Q. Hamid. 1997. Upregulation of alpha GM-CSF-receptor in nonatopic asthma but not in atopic asthma. *J. Allergy Clin. Immunol.* 99:666–672.

54. Vermaelen, K.Y., D. Cataldo, K. Tournoy, T. Maes, A. Dhulst, R. Louis, J.M. Foidart, A. Noel, and R. Pauwels. 2003. Matrix metalloproteinase-9-mediated dendritic cell recruitment into the airways is a critical step in a mouse model of asthma. *J. Immunol.* 171:1016–1022.

55. Sakai, K., A. Yokoyama, N. Kohno, H. Hamada, and K. Hiwada. 2001. Prolonged antigen exposure ameliorates airway inflammation but not remodeling in a mouse model of bronchial asthma. *Int. Arch. Allergy Immunol.* 126:126–134.